Carbon Hollow Nanospheres from Chlorination of Ferrocene

Nebil A. Katcho,[†,‡] Esteban Urones-Garrote,[§] David Ávila-Brande,[†] Adrián Gómez-Herrero,[§] Sigita Urbonaite,[∥] Stefan Csillag,[⊥] Enrique Lomba,[‡] Fernando Agulló-Rueda,[#] Angel R. Landa-Cánovas,*[,#] and L. Carlos Otero-Díaz[†,§]

Departamento de Química Inorgánica, Facultad de Ciencias Químicas, Universidad Complutense de Madrid, E-28040, Madrid, Spain, Instituto de Química Física Rocasolano, CSIC, Serrano 119, E-28006, Madrid, Spain, Centro de Microscopía, Universidad Complutense de Madrid, E-28040, Madrid, Spain, Department of Structural Chemistry, Stockholm University, S-106 91 Stockholm, Sweden, Department of Physics, Stockholm University, AlbaNova University Centre, S-106 91 Stockholm, Sweden, and Instituto de Ciencia de Materiales de Madrid, CSIC, C/Sor Juana Inés de la Cruz 3, Cantoblanco E-28049, Madrid, Spain

Received December 18, 2006. Revised Manuscript Received February 14, 2007

The chlorination of ferrocene at 900 °C yields very interesting carbon hollow nanospheres (CHNSs) with diameters of ∼50−150 nm and ∼12−25 nm thick walls. X-ray energy-dispersive spectroscopy shows no traces of chlorine or iron and the π^*/σ^* ratio of the carbon bonding was quantified by electron energy-loss spectroscopy with 80% sp^2 (100% sp^2 for pure graphite). Energy-filtered transmission electron microscopy has been used to establish the hollow nature of the CHNSs by thickness mapping. Electron energy loss spectroscopy, high-resolution TEM, and Raman microspectroscopy techniques have stated that the CHNS carbon walls are composed of disordered and independent curved graphene nanoflakes ∼3−4 nm long that tend to graphitize with longer reaction times.

Introduction

The synthesis of carbon fullerenes,[1] carbon nanotubes,[2] and carbon onions[3] in recent decades have attracted enormous interest in nanostructured carbon. It has great importance[4,5] because of the potential applications such as cold electron-field emitters,[6] gas-storage media,[7] and Li-intercalation materials for batteries.[8] Besides, the synthesis of carbon nanocapsules has practical interest because they allow the encapsulation of different materials within the empty core domain. Therefore, carbon hollow nanospheres (CHNSs) are very promising as catalyst supports,[9] in the protection of unstable organic substances,[10] and also in drug delivery.[11] CHNSs reported until now in the literature are either amorphous or graphitic, also being called carbon nanoshells.[12−15] This work is dedicated to the structural and chemical characterization of very peculiar carbon hollow nanospheres obtained by direct chlorination of ferrocene at relatively high temperature (900 °C).

The chlorination of metal carbides is now a well-established method to obtain nanostructured carbons named carbide-derived carbons (CDC).[16] This method consists of the extraction of the metal with Cl_2 by forming the volatile metal chloride, according to the reaction

$$MC_x\,(s) + (y/2)Cl_2\,(g) \rightarrow x\mathrm{C}\,(s) + MCl_y\,(g)$$

The product of the reaction is nanostructured carbon, whose structural characteristics are determined by the starting metal carbide and the chlorination reaction conditions, such as temperature and reaction time. It is considered that the initial atomic structure of the metal carbide can condition the nanostructure of the carbon formed, acting then as a template for the final product. The nature of the produced metal halide can also influence the result of the reaction. This method has been applied to a great variety of metal carbides, such as SiC, TiC, Al_4C_3, NbC, Fe_3C, and B_4C.[16−23]

Recently, a step forward was taken in applying the chlorination method to a different kind of carbon precursor

* Corresponding author. E-mail: landa@icmm.csic.es. Tel.: 34-91-3349013. Fax: 34-91-3720623.
† Departamento Química Inorgánica, F. CC. Químicas, UCM.
‡ Instituto de Química Física Rocasolano, CSIC.
§ Centro de Microscopía, UCM.
∥ Department Structural Chemistry, SU.
⊥ Department of Physics, SU.
Instituto de Ciencia de Materiales de Madrid, CSIC.

(1) Kroto, H. W.; Heath, J. R.; O'Brian, S. C.; Curl, R. F.; Smalley, R. E. *Nature* **1985**, *318*, 162.
(2) Iijima, S. *Nature* **1991**, *354*, 56.
(3) Ugarte, D. *Nature* **1992**, *359*, 707.
(4) Shenderova, O. A.; Zhirnov, V. V.; Brenner, D. W. *Crit. Rev. Solid State Mater. Sci.* **2002**, *27* (3/4), 227.
(5) Inagaki, M.; Kaneko, K.; Nishizawa, T. *Carbon* **2004**, *42*, 1401.
(6) Bonard, J. M.; Croci, M.; Klinke, C.; Kurt, R.; Noury, O.; Weiss, N. *Carbon* **2002**, *40*, 1715.
(7) Schlapbach, L.; Züttel, A. *Nature* **2001**, *414*, 353.
(8) Maurin, G.; Bousquet, C.; Henn, F.; Bernier, P.; Almairac, R.; Simon, B. *Chem. Phys. Lett.* **2002**, *312*, 14.
(9) Mathiowitz, E.; Jacob, J. S.; Jong, Y. S.; Carino, G. P.; Chickering, D. E.; Chaturvedi, P.; Santos, C. A.; Vijayaraghavan, K.; Montgomery, S.; Bassett, M.; Morrell, C. *Nature* **1997**, *386*, 410.
(10) Haiyong, H.; Remsen, E. E.; Kowalewski, T.; Wooley, K. L. *J. Am. Chem. Soc.* **1999**, *121* (15), 3805.
(11) Gill, I.; Ballesteros, A. *J. Am. Chem. Soc.* **1998**, *128* (34), 8587.
(12) Wang, Z. L.; Yin, J. S. *Chem. Phys. Lett.* **1998**, *289*, 189.
(13) Cowley, J. M.; Kiang, C. H. *Carbon* **2000**, *38*, 1437.
(14) Ni, Y.; Shao, M.; Tong, Y.; Qiang, G.; Wei, X. *J. Solid State Chem.* **2005**, *178*, 908.
(15) Chu, C.; Hwang, G.; Chiou, J.; Pong, W.; Lin, C.; Tsai, C.; Lin, H.; Chang, Y.; Chang, C.; Hsu, A. H.; Huang, W.; Guo, J.; Chen, P.; Luh, T. *Adv. Mater.* **2005**, *17*, 2707.
(16) Gogotsi, Y.; Welz, S.; Ersoy, D. A.; McNallan, M. J. *Nature* **2001**, *411*, 283.
(17) Welz, S.; Gogotsi, Y.; McNallan, M. J. *J. Appl. Phys.* **2003**, *93*, 4207.

10.1021/cm062997w CCC: $37.00
Published on Web 04/04/2007

such as metallocenes. Thus, Ávila-Brande et al.[24] have shown that the chlorination of metallocenes gives rise to different nanostructured carbons compared to the chlorination of metal carbides, but in the former case it seems that the nature of the formed metal chloride has a more important effect than the atomic structure of the starting metallocene. Urones-Garrote et al.[25] reported the synthesis and characterization of different carbon nanostructures by the chlorination of ferrocene at different temperatures. They observed amorphous carbon nanotubes at low temperatures (200 °C) but carbon "nanobags" at higher temperatures.

In this work we report the synthesis and structural characterization of carbon hollow nanospheres produced by chlorination of ferrocene at 900 °C.

Experimental Section

Samples were prepared by direct reaction of ferrocene −Fe-$(C_5H_5)_2$−, placed in 6 cm long quartz boats inside a tubular furnace, under a flow of pure Cl_2 at 900 °C for 30 min (sample A) and 3 h (sample B), according to the following reaction:

$$Fe(C_5H_5)_2\,(s) + {}^{13}/_{2}Cl_2\,(g) \rightarrow FeCl_3\,(g) + 10HCl\,(g) + 10C\,(s)$$

The flow of excess Cl_2 gas in the quartz tube was maintained while raising and lowering the temperature. The exiting gases (volatile iron chlorides, HCl, and Cl_2) were neutralized in NaOH concentrated solutions at the exit of the tubular furnace.

The samples were studied by X-ray powder diffraction (XRPD) with a Siemens D-501 diffractometer (Cu Kα_1 radiation, λ = 0.15406 nm). Transmission electron microscopy (TEM) was carried out in a Philips CM200FEG (field emission gun) microscope operating at 200 kV acceleration voltage and fitted with an EDAX DX4 spectrometer for X-ray energy-dispersive spectroscopy (XEDS). For electron energy-loss spectroscopy (EELS) experiments this microscope is equipped with a GIF 200 energy filter with an energy resolution of 0.95 eV. High-resolution TEM (HRTEM) images were acquired in a JEM 3000F microscope operating at 300 kV acceleration voltage with a point resolution of 0.17 nm. TEM samples were prepared from ultrasonic dispersions of the carbon powders in acetone. One drop of each suspension was deposited over a copper grid covered with a holey carbon film.

Low-temperature nitrogen adsorption experiments were performed at the boiling point of nitrogen using Surface Area and Porosity Analyzer ASAP2020 (Micromeritics). The specific surface area of the carbon material was calculated according to BET theory. The microporous fraction is evaluated using t-plot. Pore size distribution (PSD) calculations were made using (N_2) original DFTplus software from Micromeritics. For comparison, the Howarth-Kawazoe and BJH methods for determination of pore size were used as well.

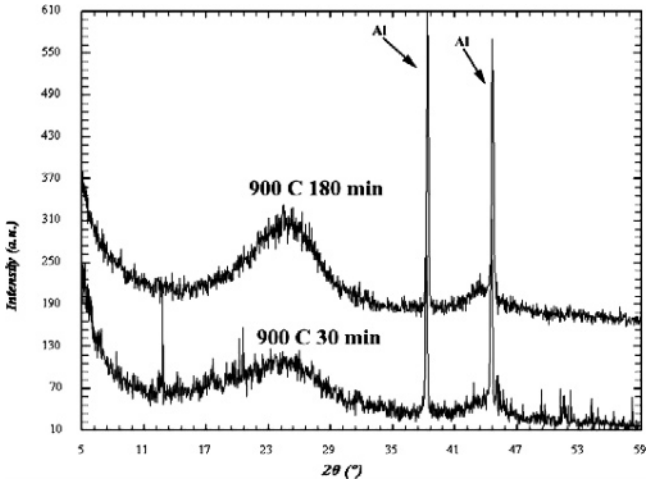

Figure 1. X-ray powder diffraction patterns from sample A (900 °C, 30 min) and sample B (900 °C, 3 h). Sharp aluminum peaks are rising from the aluminum holder. Two broad maxima appear at $2\theta \sim 24°$ and $43-44°$ which correspond to graphite 002 and 101 reflections.

Raman spectra were acquired with a Renishaw Ramascope 2000 microspectrometer for an excitation wavelength of 514.5 nm. The spectral resolution was 4 cm^{-1} and the spatial resolution 0.6 μm.

Results and Discussion

The powder X-ray diffraction pattern from sample A (see Figure 1) shows two very broad bands observed at $2\theta \sim 24°$ and $2\theta \sim 43-44°$, although the last one is partially hidden by aluminum reflections coming from the sample holder. They appear at the same reciprocal spacings than 002 and 101 graphite reflections respectively but their broadness already indicates the disorder of the sample.

However, transmission electron microscopy allows us to obtain direct information about the nanostructured nature of these carbon materials. TEM micrographs (see Figure 2a) show that these carbon species consist of very homogeneous spherical particles with an average diameter of ∼50−150 nm. XEDS analyses from these carbon nanoparticles only denote the presence of carbon, indicating that iron and chlorine have been completely eliminated. These spherical particles present a lighter contrast in the center, probably indicative of a hollow core because, in compositionally homogeneous disordered materials, changes in contrast suggest a change in the thickness because no diffraction contrast would be present. The darker contrast of the rims would correspond to the walls of the hollow particle, the thickness of these walls being around 12−25 nm.

High-resolution TEM (HRTEM) images from these CHNSs, Figures 2b and 2c, indicate that the carbon walls consist of either amorphous or disordered carbon, without the presence of stacked graphitic layers, but very little extra information can be obtained about the nature of the carbon forming the walls of these particles because the lack of any periodicity in the images greatly complicates their interpretation.

Energy-filtered TEM (EFTEM) has been used to confirm that the spheres are hollow. For this purpose, a 10 eV energy window has been used to obtain a filtered image from the

(18) Chen, X.; Cantrell, D. R.; Kohlhaas, K.; Stankovich, S.; Ibers, J. A; Jaroniec, M.; Gao, H.; Li, X.; Ruoff, R. S. *Chem. Mater.* **2006**, *18*, 753.
(19) Zheng, J.; Ekström, T. C.; Gordeev, S. K.; Jacob, M. *J. Mater. Chem* **2000**, *10*, 1039.
(20) Leis, J.; Perkson, A.; Arulepp, M.; Käärik, M.; Svensson, G. *Carbon* **2001**, *39*, 2043.
(21) Ávila-Brande, D.; Katcho, N. A.; Urones-Garrote, E.; Gómez-Herrero, A.; Landa-Cánovas, A. R.; Otero-Díaz, L. C. *Carbon* **2006**, *44*, 753.
(22) Dimovski, S.; Nikitin, A.; Ye, H.; Gogotsi, Y. *J. Mater. Chem.* **2004**, *14*, 238.
(23) Dash, R. K.; Nikitin, A.; Gogotsi, Y. *Microporous Mesoporous Mater.* **2004**, *72*, 203.
(24) Ávila-Brande, D.; Urones-Garrote, E.; Katcho, N. A.; Lomba, E.; Gómez-Herrero, A.; Landa-Cánovas, A. R.; Otero-Díaz, L. C. *Micron* **2007**, *38*, 335.
(25) Urones-Garrote, E.; Ávila-Brande, D.; Ayape-Katcho, N.; Gómez-Herrero, A.; Landa-Cánovas, A. R.; Otero-Díaz, L. C. *Carbon* **2005**, *43*, 978.

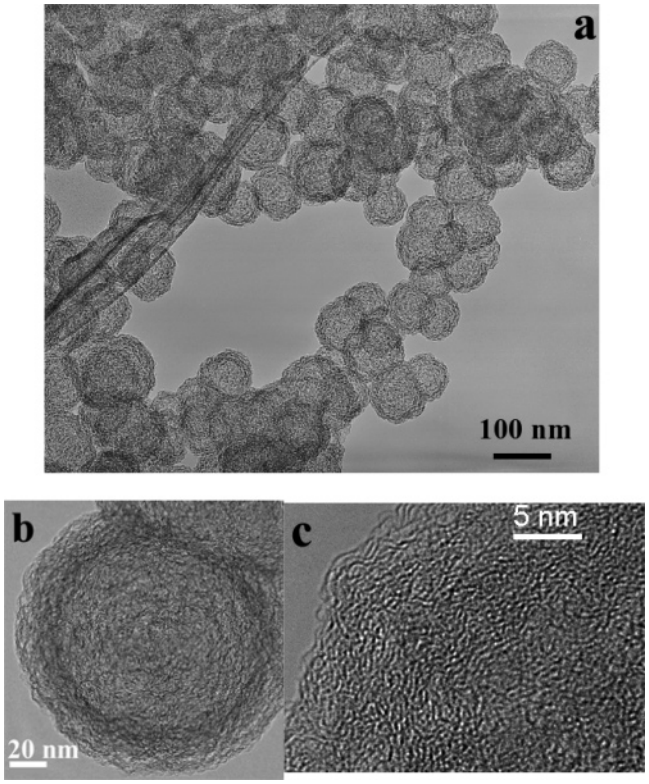

Figure 2. Transmission electron micrograph (TEM) of carbon particles from sample A. (a) General view of the sample at low magnification. (b) TEM image of a single carbon hollow nanosphere. (c) Detail from the disordered carbon wall of the hollow sphere.

plasmon loss region (image formed only with the inelastic electrons) and from the zero-loss peak (image formed only with elastically scattered electrons). The fraction between these two images will produce another image whose contrast is directly related to the thickness of the sample through the inelastic mean free path parameter.[26] In Figure 3a we present a TEM micrograph with carbon spherical particles from sample A. Figure 3b shows the corresponding EFTEM thickness map. The intensity profile of the image has been measured across the white line depicted in the figure and the intensity variations are represented in Figure 3c. In the graphic we observe a rapid increment of the thickness because we are scanning the intensity of the hollow sphere wall. Then, a rapid decrease is produced because we pass the wall limit. Finally, the intensity is more or less kept constant because we are now scanning just the upper and lower walls which are almost perpendicular to the electron beam, so the observed thickness almost does not vary and it would correspond to twice the wall thickness.

EELS experiments were carried out to obtain more information about the nature of these carbon hollow spheres. ELNES (energy-loss near-edge structure) spectra corresponding to the carbon-K absorption edge are characteristic of amorphous or disordered carbon, showing the typical π^* and σ^* peaks. However, when these spectra were obtained with a small condensed electron probe located at the wall and at the center of the hollow sphere, they clearly show a different π^*/σ^* ratio depending on the different area where they were

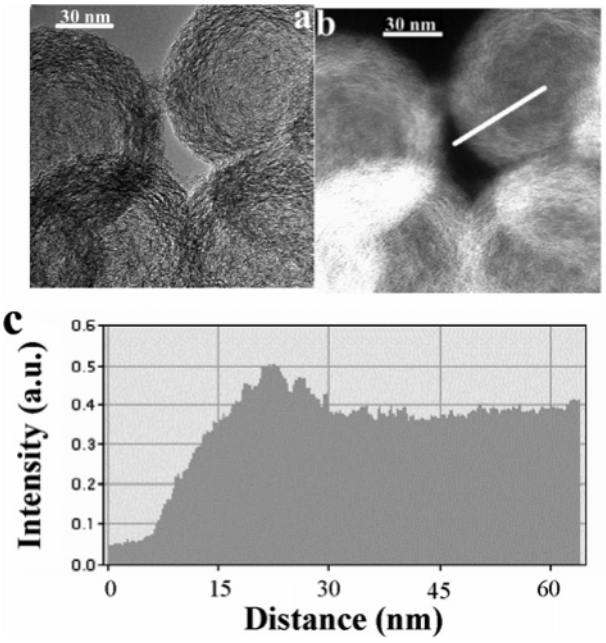

Figure 3. (a) Elastic image of carbon hollow spheres obtained by selecting the elastically scattered electrons from the zero-loss peak with a 10 eV wide window. (b) Thickness map processed by dividing the inelastically filtered image (by selecting the plasmon electrons with a 10 eV window) by the elastically filtered image. (c) Thickness profile obtained by scanning the observed intensity along the white line depicted in Figure 2b.

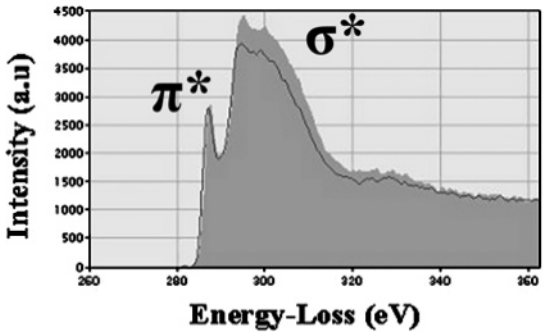

Figure 4. ELNES profiles obtained from the edges (outlined) and from the center (filled) of a carbon hollow sphere. Notice the difference in the π^*/σ^* ratio.

collected from because the relative intensity of π^* and σ^* maxima is related in this case to the anisotropy of the sample[26] (see Figure 4). Therefore, ELNES spectra demonstrate that the carbon forming these hollow nanospheres is not amorphous because it must have a certain structure to give rise to the proven anisotropy. Consequently, from now on we must refer to these particles as composed of disordered instead of amorphous carbon, being composed of graphene layers arranged perpendicular to the sphere radius. Since the π^* contribution increases at the wall of the CHNSs, they must consist of some arrangement of graphene layers with some preferential orientation perpendicular to the sphere radius because the walls always give rise to a more intense π^* peak; therefore, the graphene layers are parallel to the beam.

However, if the spectra were acquired in the "magic angle" condition, they would not vary with the specimen orientation.[27] The magic angle is a function of the collection angle

(26) Egerton, R. F. *Electron Energy-Loss Spectroscopy in the Electron Microscope*; Plenum Press: New York, 1996.

(27) Menon, N. K.; Yuan, J. *Ultramicroscopy* **1998**, *74*, 83.

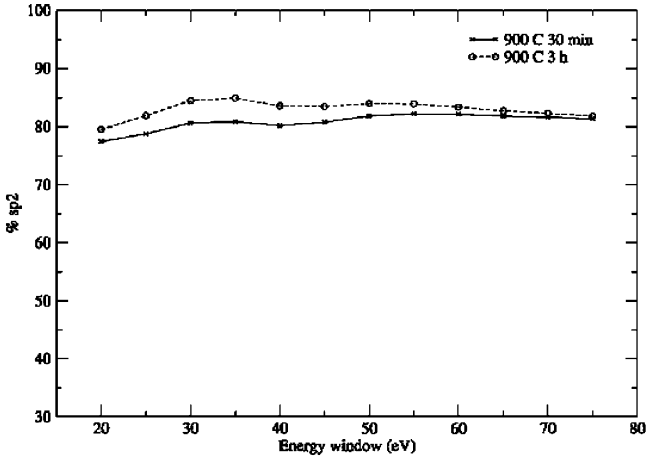

Figure 5. Quantification of the sp^2/sp^3 ratio in the CHNSs versus the different window energy widths used for the quantification.

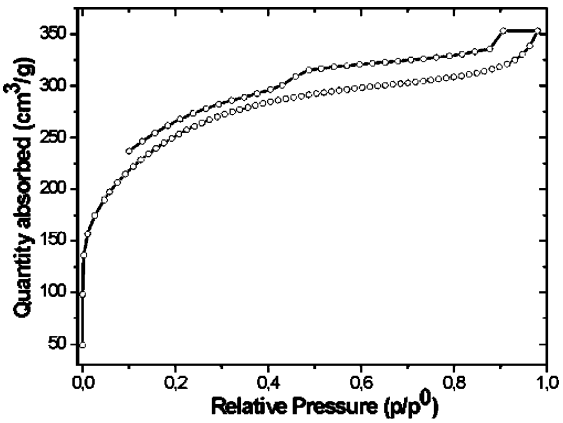

Figure 6. BET isotherm linear plot for sample A.

(β) and convergence semiangle (α) of the incident electrons on the specimen and is approximately 2 times the C−K edge characteristic scattering angle.[28] To avoid anisotropy effects, we acquired EELS spectra at magic angle condition to quantify the real π^*/σ^* ratio of the carbon material. This condition for the C−K edge in the Philips CM200 FEG microscope is fulfilled for a collection angle of $\beta \sim 1.7$ mrad. To calculate the sp^2-bonding proportion in the sample, we have used the method proposed by Titantah and Lamoen.[29] This method consists of fitting the C−K ELNES of the sample to an ab initio calculation of the π^* contribution in graphite. Experimental spectra from graphite were used as standard for which the percentage of sp^2 is 100%. The obtained sp^2 contribution is ranging between 77 and 80%, being almost independent of the size of the energy window used in the quantification (Figure 5).

The isotherm plot obtained for sample A (see Figure 6) corresponds to the H4 type.[30] The hysteresis loop does not terminate in a plateau at high $p/p°$, it does not close at $p/p° < 1$, and its limiting desorption boundary curve is dependent on the experimental conditions. No closing hysteresis loops are often given by the aggregates of platy particles. The sample presents high surface area ($S_a = 924$ m^2/g). The total pore volume is 0.55 cm^3/g and the micropore volume is 0.11 cm^3/g. The pore size distribution (Figure 7) calculated using (N_2) original density functional theory (DFT) model assuming slit pore geometry evidence micro- and mesoporosity. Compared to the H−K method, we see that the width of the micropores agrees in both methods. BJH desorption gives an average pore width of 2.9 nm, which is in agreement with the DFT calculated pore width of mesoporous part of PSD. These porosities are found in the walls of the spheres because the sizes of the mesopores (2−4 nm) are too small to be explained as voids between spheres with diameters of 50−100 nm.

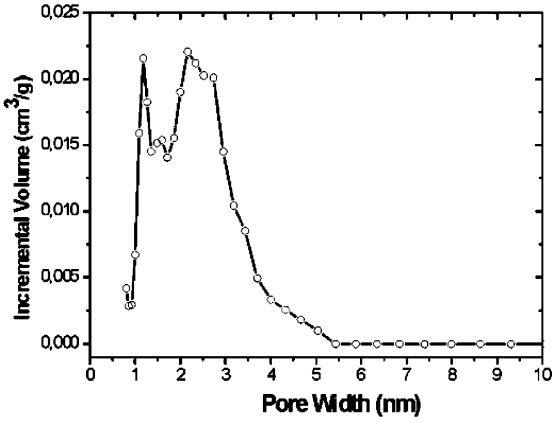

Figure 7. Pore size distribution curve obtained for sample A.

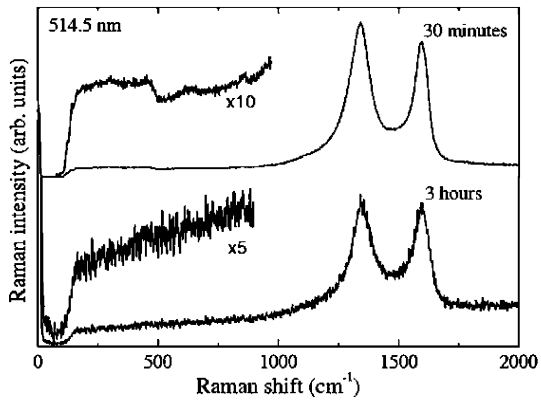

Figure 8. Raman spectra obtained for sample A (30 min**)** and for sample B (3 h**)**.

The structure of carbon materials can be investigated by Raman spectroscopy in a detailed way to characterize the bonding, order, and crystallite or domain size. The Raman spectrum of Figure 8 is typical of disordered graphitic materials with two Raman bands, one at about 1593 cm^{-1} due to the E_{2g} in-plane phonon modes of graphene layer (E_{2g}),[31] usually named as "G" peak, and another at about 1339 cm^{-1}, designated as "D", which is due to disorder in the graphene layers.[32] The frequency of the G band, which is sensitive to changes in the structure,[33] corresponds to "nanocrystalline graphitic material" and with low proportion of sp^3-bonded carbon. Also the width of the G band[33] (see Table 1) indicates that the material is formed by graphene nanoflakes of a size of about 3−4 nm. This value can be

(28) Daniels, H.; Brown, A.; Scott, A.; Nichells, T.; Rand, B.; Brydson, R. *Ultramicroscopy* **2003**, *96*, 523.
(29) Titantah, J. T.; Lamoen, D. *Phys. Rev. B* **2004**, *70*, 075115.
(30) Sing, K. S. W.; Everett, D. H.; Haul, R. A. W.; Moscou, L.; Pierotti, R. A.; Rouquerol, J.; Siemieniewska, T. *Pure Appl. Chem.* **1985**, *57*, 603.
(31) Tuinstra, F.; Koenig, J. L. *J. Chem. Phys.* **1970**, *53*, 1126.
(32) Robertson, J. *Mater. Sci. Eng. Rep.* **2002**, *37*, 129.
(33) Ferrari, A. C.; Rodil, S. E.; Robertson, J. *Phys. Rev. B* **2003**, *67*, 155306.

Table 1. Parameters Quantified from Raman Spectra of Samples A and B

	sample A (30 min)	sample B (3 h)
ν_D (cm^{-1})	1339.25	1349
ν_G (cm^{-1})	1593.41	1593
Γ_D (cm^{-1})	122.04	134
Γ_G (cm^{-1})	67.81	83
$I_{int}(D)$	960281.01	44096
$I_{int}(G)$	467524.12	26091
$I_{max}(D)$	5009.42	263
$I_{max}(G)$	4389.23	251
$I_{max}(D)/I_{max}(G)$	1.14	1.048

measured with higher precision from the ratio between the two bands G and D according to the expression

$$I_{max}(D)/I_{max}(G) = C(\lambda)/L$$

L being the size of the graphene nanoflakes and $C = 4.4$ nm for $\lambda = 514.5$ nm. From these values the size of the crystallites is $L = 3.9$ nm.

The Raman spectrum also presents a weak and broad band at low frequencies. The origin of this band is not clear and it is beyond the scope of the present contribution, but it should be noted that single-walled carbon nanotubes present discrete bands due to radial breathing modes at these frequencies.[34,35]

To check the evolution of the sample, another one was prepared with a longer reaction time (3 h, sample B). X-ray powder diffraction indicates a higher degree of graphitization because the graphitic reflections are more intense and less broad than those in sample A. BET measurements showed a lower value for the surface area ($S_a = 809$ m^2/g) with a decrease of 12.4% with respect to sample A. TEM microscopy demonstrated that the sample is still composed of hollow carbon nanospheres (Figure 9a). ELNES π^*/σ^* ratio quantification produces a 80−85% sp^2-bonding contribution for sample B, slightly higher than that in sample A. HRTEM shows very distinct characteristics now. In Figure 9b we present a high-resolution micrograph from one sample B hollow nanosphere. In the wall, we can clearly distinguish small platelets composed of the graphitic stacking of two to five curved graphene layers 3−5 nm long. The Raman spectra of this sample are noisier since the higher graphitization of the sample makes it a better conductor and therefore with worse light transmission (see Figure 8 and Table 1). With respect to the D and G bands, they are wider for this sample when compared to those of sample A. The G band appears at 1539 cm^{-1}, as in sample A, whereas the D band shifts up to 1349 cm^{-1}. From the D/G intensity ratio we obtain a graphene nanoflake size $L = 4.2$ nm, slightly bigger than that in sample A.

Raman results indicate that sample A is composed of graphene nanoflakes but ELNES shows that its sp^2-bonding percentage decreases compared with that of standard graphite. One reason for this could be the curvature of graphene nanoflakes that would provoke a change in the carbon hybridation from sp^2 to $sp^{2+\delta}$,[29] giving rise to a decrease of

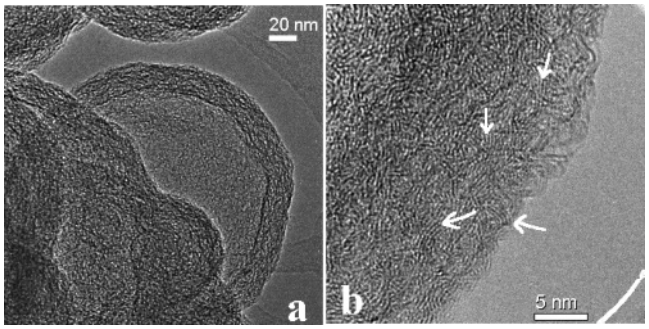

Figure 9. TEM images from CHNSs (sample B) at medium (a) and high resolution (b). Notice how four or five curved graphene nanoflakes stack in platelets ~4 nm long.

π contribution to the spectrum. Besides, extra σ-bonding could happen between terminal carbons of different nanoflakes, changing the π^*/σ^* ratio.

The comparison of the results obtained for samples A and B is interesting. From TEM and Raman spectroscopy we deduced that the CHNSs from both samples are composed of graphene nanoflakes that tend to stack in the sample B case. Due to the higher reaction time, the sample B nanoflakes are slightly bigger and bonding quantification by ELNES gives a slightly higher percentage of π-bonding. The stacking of the carbon nanoflakes could implicate a reduction of their curvature and, therefore, an improvement of the overlapping of the p_z orbitals, consequently increasing the π contribution. Besides, longer reaction times could act as a kind of annealing favoring the formation of bigger graphene nanoflakes and relatively less carbon atoms would be located at the edges. Then, it would decrease the possibility of interflake σ-bonding.

The nanostructure observed in these carbons could induce one to consider them as nongraphitizing carbons[36,37] because higher reaction times tend to produce small arrays of stacked graphene nanoflakes, being quite misoriented with respect to the surrounding ones. Therefore, higher reaction times could act in a way similar to higher temperature treatment. However, the preferential perpendicularity of the nanoflakes of sample A to the sphere radius, demonstrated by ELNES experiments, could induce one to expect the opposite because it is proposed that the relative preferential orientation of graphene layers could induce the graphitizing of the sample.[37] Nonetheless, we have to consider that higher reaction times cannot be directly compared to the high-temperature treatments necessary to elucidate this question.

Finally, it has already been suggested[25] that in the chlorination reaction of ferrocene, carbon transport could be responsible for the creation of open carbon morphologies such as amorphous carbon nanotubes or the carbon hollow nanospheres described here. Anyway, the mechanism of formation of these CHNSs still remains an open question. It has already been proposed in refs 24 and 25 that the first step in the chlorination of metallocenes is the formation of amorphous solid spheres composed of carbon, metal, and chlorine. It is feasible that at 900 °C the metal chloride ($FeCl_3$ in this case) diffuses in all directions to the surface of the

(34) Rao, A. M.; Richter, E.; Bandow, S.; Chase, B.; Eklund, P. C.; Williams, K. A.; Fang, S.; Subbaswamy, K. R.; Menon, M.; Thess, A.; Smalley, R. E.; Dresselhaus, G.; Dresselhaus, M. S. *Science* **1997**, *275*, 187.
(35) Dresselhaus, M. S.; Eklund, P. C. *Adv. Phys.* **2000**, *49*, 705.
(36) Franklin, R. E. *Proc. R. Soc. London, Ser. A* **1951**, *209*, 196.
(37) Harris, P. J. F. *Carbon nanostructures and related structures*; Cambridge University Press: Cambridge, 1999.

sphere, probably transporting carbon in the process. When $FeCl_3$ reaches the surface, it would leave the sphere, depositing the carbon and, therefore, forming in the end a carbon crust with a holey interior, i.e., a CHNS.

The possibility remains open that iron could play a role in the making of the hollow carbon spheres. However, we have found no evidence at all by TEM of the presence of iron metallic particles that could catalyze the growth of the hollow spheres in a way similar to that occurring in the catalytic synthesis of carbon nanotubes. In other samples prepared at lower temperatures we found iron always associated to chlorine.

Conclusions

A new kind of carbon hollow nanospheres (50−150 nm diameter) with 12−25 nm thick walls has been synthesized by the chlorination of ferrocene at 900 °C. Although at first sight the walls seem to be composed of amorphous carbon they are actually formed by a disordered array of independent curved graphene nanoflakes (∼4 nm diameter) as the combined interpretation of TEM, EELS, and Raman spectra suggest. If higher reaction times are used, like in sample B, the structure of the CHNS walls seem to evolve to nanocrystalline graphite with no more than five graphene layers stacked and still visibly bent.

Acknowledgment. The authors are thankful for financial support from the UCM-Santander project with reference PR 27/05-13982.

CM062997W